Magic Rydberg-Rydberg transitions in electric fields

Michael Peper,[*] Johannes Deiglmayr,[†] and Frédéric Merkt [‡]
Laboratory of Physical Chemistry, ETH Zürich, 8093 Zürich, Switzerland

Carla Sanna and H. B. van Linden van den Heuvell
Van der Waals-Zeeman Institute, Institute of Physics, University of Amsterdam, Science Park 904, 1098 XH Amsterdam, The Netherlands

Rydberg states of atoms and molecules are very sensitive to electric fields. This property makes them ideal electric-field sensors but is detrimental to applications of Rydberg states in quantum optics, quantum-information processing, and quantum simulation because of inhomogeneous Stark broadening and the resulting loss of quantum coherence. We demonstrate, with the example of Rydberg states of ^{39}K, the existence of Rydberg-Rydberg transitions with extremely small differential dc Stark shifts, which we call *dc-field-magic Rydberg-Rydberg transitions*. These transitions hardly exhibit any Stark broadening, even when the electric-field strength varies by as much as 10 V cm^{-1} over the experimental volume. We present a systematic study of dc-field-magic Rydberg-Rydberg transitions combining experiment and calculations and classify them in three main types, which should also be encountered in the other alkali-metal atoms, in alkaline-earth-metal atoms, and even in molecules. The observed insensitivity to dc electric fields does not reduce the interactions between Rydberg atoms, even if they are dominantly electric dipole-dipole in nature. Rydberg states coupled by dc-field-magic Rydberg-Rydberg transitions, therefore, have great potential as qubits.

I. INTRODUCTION

Rydberg atoms have very attractive properties for experiments in quantum optics, quantum-information processing, and quantum simulation [1–8]: They exhibit large electric dipole moments that can be used to tailor the interaction between two or more atoms, entangle them using the dipole-blockade effect, realize quantum gates, and generate Rydberg-atom samples exhibiting long-range order. In field-free space, Rydberg atoms display long coherence times, which makes them attractive as components of hybrid quantum systems combining the advantages of solid-state devices and atoms in the gas phase [6,9–16].

Rydberg atoms are also very sensitive to electric fields. The polarizability of penetrating low-l Rydberg states scales with the principal quantum number as n^7 [17]. Nonpenetrating Rydberg states, for which all states of a given value of n are degenerate in field-free space, exhibit a linear Stark effect and large dipole moments that scale as n^2. This sensitivity makes Rydberg atoms ideal sensors for electric fields [18–21]. At the same time, it severely limits their use in several of the quantum-optics and quantum-information-processing experiments listed above. Indeed, inhomogeneous electric fields broaden the transitions and reduce the coherence times.

The effects of inhomogeneous stray fields become particularly virulent in experiments which aim at manipulating Rydberg atoms near chip surfaces [6,9,11–14,16,22,23]. Patch potentials, adsorbates, and electrical insulators on the chip surfaces typically give rise to electric fields varying in the range up to about 10 V cm^{-1} at distances from the surfaces where the atoms are trapped and/or manipulated [6,11,12,14,22,24]. The challenge is to exploit the interactions of the strongly dipolar Rydberg atoms with other atoms or quantum dots integrated on the chip surface without suffering from their sensitivity to electric fields. Several approaches have been followed to meet this challenge. Hyafil *et al.* [9], Mozley *et al.* [10], Jones *et al.* [25], and Ni *et al.* [26] have proposed using circular Rydberg states, which are intrinsically insensitive to electric fields, and exploiting microwave fields to dress the atoms so as to cancel their remaining first- and second-order dependence on electric fields. Hermann-Avigliano *et al.* [15] have demonstrated how to reduce stray fields emanating from superconducting circuits by covering the chip surface with a thin metallic layer, thus achieving coherence times on the millisecond timescale for Rydberg-Rydberg transitions of Rb (see also Ref. [27]). Thiele *et al.* [21] have shown how to measure and compensate three-dimensional electric-field distributions near surfaces. Although these approaches have had some success, inhomogeneous stray fields still hamper progress in this field.

In this paper, we propose and demonstrate an alternative method to overcome the difficulties arising from stray electric fields in quantum-optics experiments with Rydberg atoms. Rather than eliminating the electric stray fields, or reducing the field sensitivity of specific Rydberg states by microwave dressing, we identify *field-insensitive Rydberg-Rydberg transitions*, i.e., transitions between two Rydberg states exhibiting close-to-identical Stark effects. Our strategy is the dc Stark equivalent of the strategy, now widely used in metrology,

---

[*]michael.peper@phys.chem.ethz.ch

[†]Present address: University of Leipzig, Felix-Bloch Institut, 04103 Leipzig, Germany.

[‡]merkt@phys.chem.ethz.ch

based on the use of "magic wavelengths" [28] to cancel ac Stark shifts in optical traps. More generally, it is also related to "magic angles" used, e.g., in magnetic resonance experiments to suppress inhomogeneous broadenings caused by anisotropic spin-spin interactions [29]. Magic angles and magic wavelengths correspond to a maximal insensitivity to an inhomogeneous broadening mechanism and are found by adjusting a free parameter (an angle or a wavelength). In contrast, the Rydberg-Rydberg transitions that we introduce here to suppress dc Stark broadenings are intrinsically field independent and do not require the tuning of external adjustable parameters. The parameters we tune are internal (physical) properties of the Rydberg-Stark states involved in the transitions, i.e., their dipole moments and their polarizabilities. Because the state density rapidly increases with n, these properties become quasicontinuous at sufficiently high n values, which guarantees that one always finds field-insensitive transitions. We therefore call the field-insensitive Rydberg-Rydberg transitions that are at the heart of our approach "dc-field-magic Rydberg-Rydberg transitions". The results we present were obtained on Rydberg states of potassium (^{39}K), but we have verified, through calculations, that the same behavior will also be encountered in the other alkali-metal atoms, in alkaline-earth-metal atoms, and even in molecules.

In the following, we label low-l Rydberg states of K subject to the quadratic Stark effect as $(n, l, j, |m_j|)$, where n, l, and j are the principal, orbital, and total angular-momentum quantum numbers, respectively, and $|m_j|$ is the absolute value of the projection quantum number along the electric-field vector. We label high-l Rydberg-Stark states as $(n, k_{\text{eff}}, j^{+/-}, |m_j|)$, where k_{eff} is an index giving the slope of the Stark state when its energy is plotted against the electric-field strength, and $j^{+/-}$ designates the upper ($+$) or lower ($-$) fine-structure state. k_{eff} is smaller than the hydrogenic k label [17] by the number of penetrating low-l states. For example, $k_{\text{eff}} = k - 3$ in the case of K ($|m_j| = 1/2$) Rydberg states, because s, p, and d Rydberg states are not yet strongly mixed with nonpenetrating states for the electric-field and n ranges of interest.

II. CALCULATION OF STARK SHIFTS AND IDENTIFICATION OF MAGIC TRANSITIONS

To calculate the energy-level structure of K Rydberg states in electric fields, we use the procedure described by Zimmerman et al. [30] and determine the eigenvalues of the Hamiltonian,

$$\hat{H} = \hat{H}_0 + eF\hat{z}, \tag{1}$$

where $\hat{H}_0$ is chosen as a diagonal matrix with elements given by Rydberg's formula,

$$E_0(n, l, j) = E_{\text{I}} - \frac{hcR_{\text{K}}}{[n - \delta_{l,j}(n)]^2}. \tag{2}$$

In Eq. (2), the effects of the spin-orbit interaction are included in the energy-dependent quantum defects as listed in Ref. [31]. The off-diagonal elements arising from the Stark operator $eF\hat{z}$ are determined as integrals of the form

$$\langle n, l, j, m_j | eF\hat{z} | n', l', j', m_j' \rangle = eF \mathcal{R}_{n,l,j,n',l',j'} \mathcal{G}_{l,j,m_j,l',j',m_j'}, \tag{3}$$

where $\mathcal{G}_{l,j,m_j,l',j',m_j'}$ and $\mathcal{R}_{n,l,j,n',l',j'}$ represent the angular and radial parts of the integrals, respectively. The radial wave functions $R_{n,l}(r)$ are determined by applying Numerov's method at the eigenenergies of $\hat{H}_0$ [Eq. (2)] using the model potential $V_l(r)$ of the K$^+$ core reported by Marinescu et al. [32], to which a spin-orbit coupling term,

$$V_{\text{SO}}(r) = \frac{\hbar^2}{4m_e^2 c^2 r} \left(\frac{dV_l(r)}{dr} \right) [j(j+1) - l(l+1) - s(s+1)] \tag{4}$$

is added. The numerical convergence of the eigenvalues was checked by systematically extending the size of the n, l, j basis and the point density of the integration grid. Final calculations were performed with the full l, j basis including levels from $n = 13$ to $n = 105$. To identify magic transitions between Rydberg states i (unprimed quantum numbers) and f (primed quantum numbers), we calculated the transition frequencies $\nu_{i,f}$ and their standard deviation $\sigma_{i,f}$ in the electric-field range from 0 to 10 V cm^{-1} (0 to 1 V cm^{-1}) for all possible transitions involving states with n in the range from 20 to 50 (50 to 90) and sorted the transitions in order of increasing standard deviation. Analysis of the transitions with the lowest $\sigma_{i,f}$ values led to a classification of the most magic transitions in three types illustrated in panels (a)–(c) of Fig. 1 and referred to below as types I—III, respectively.

(1) Type-I magic transitions involve low-l states having similar polarizabilities and, thus, similar quadratic Stark shifts. Because the polarizabilities increase with l and scale as n^7 for a given l value, these transitions fulfill

$$\frac{\alpha_{l'}}{\alpha_l} = \frac{\alpha_l^* n'^7}{\alpha_l^* n^7} \approx 1, \tag{5}$$

which implies $n' < n$ for $l' > l$. In Eq. (5), α_l^* is the n-independent scaled polarizability of the l series. For the $21p_{1/2} \leftrightarrow 21s_{1/2}$ transition depicted in Fig. 1(a), the standard deviation is only 307 kHz in the range of 0–10 V cm^{-1}, whereas the maximal Stark shift $\Delta E_{\text{Stark}}^{\text{max}}/h$ of the states involved in the transition is 10.790 MHz. The Stark shift of the transition is, thus, reduced by a factor of $\Delta E_{\text{Stark}}^{\text{max}}/(h\sigma_{21p,21s})$ of about 30 compared to the Stark shifts of the levels connected by the transition.

(2) Type-II magic transitions involve linearly shifted Stark states having similar electric dipole moments, i.e., $\Delta\mu_{\text{el}} = nk_{\text{eff}} - n'k_{\text{eff}}' \approx 0$. The $(38, 12, j^-, 1/2) \rightarrow (35, 13, j^-, 1/2)$ transition used as an example of this magic-transition type in Fig. 1(b) has a σ value of 282 kHz in the field range from 3.5 to 10 V cm^{-1} and a $\Delta E_{\text{Stark}}^{\text{max}}/h$ value of 9220 MHz. The Stark-shift reduction factor $\Delta E_{\text{Stark}}^{\text{max}}/(h\sigma)$ is 32 700 in this case. The dipole mismatch $\Delta\mu_{\text{el}}$ of 1 (in atomic units, i.e., ea_0) between these two states would lead to a linear Stark shift of the transition frequency of 20 MHz at a field of 10 V cm^{-1}. This shift, however, is almost exactly compensated by higher-order Stark shifts.

(3) Type-III magic transitions involve Stark states that both have $k_{\text{eff}} = 0$ and zero dipole moments. The example presented in Fig. 1(c) involves the $(42, 0, j^+, 3/2) \rightarrow (40, 0, j^+, 1/2)$ transition, which has a σ value of 1.4 MHz in the field range from 0 to 10 V cm^{-1} and a value of $\Delta E_{\text{Stark}}^{\text{max}}/h$ of 90 MHz. $\Delta E_{\text{Stark}}^{\text{max}}/h\sigma$ is, thus, 64.
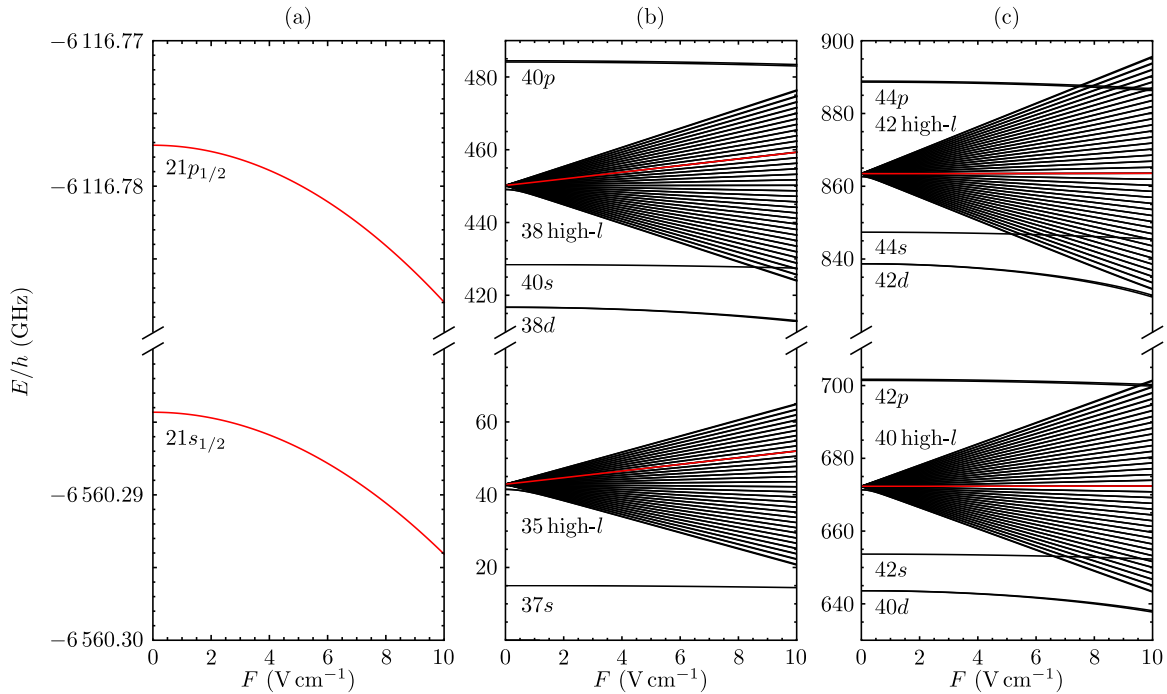
FIG. 1. Energy-level diagram of Rydberg-Stark states of ^{39}K as a function of the electric field. The Rydberg states involved in types I–III magic transitions are depicted in red in panels (a)–(c), respectively. The origin of the energy scale corresponds to the position of the $35d_{5/2}$ Rydberg state. See the text for details.

III. EXPERIMENT

To verify these predictions, the field-independent Rydberg-Rydberg transitions of ^{39}K were studied experimentally by millimeter-wave spectroscopy. Samples of ultracold ^{39}K atoms were prepared in a magneto-optical trap (MOT) as described in Refs. [31,33]. Rydberg states of ^{39}K were populated through one-photon transitions from the $4s_{1/2}(F = 1)$ ground state using a frequency-tunable single-mode continuous-wave UV laser at 285 nm [33]. The ring dye laser used to generate the UV radiation by frequency doubling was locked to an external reference cavity (Thorlabs SA200-5B), and its frequency was measured using a wavelength meter (HighFinesse WS7-60).

The millimeter-wave radiation used to record Rydberg-Rydberg transitions of ^{39}K was obtained by harmonic generation of the output of a radio-frequency generator (Anristu MG3692A) using active 18-fold (170–250 GHz, Virginia Diodes WR-9.0 with Virginia Diodes WR4.3×2) or 36-fold (350–500 GHz, Virginia Diodes WR-9.0 with Virginia Diodes WR4.3×2 and WR2.2×2) multipliers. The population transfer between the Rydberg states induced by the millimeter-wave radiation was detected state selectively by pulsed field ionization.

Electric fields with strengths in the range from 0 to 10 V cm^{-1} and direction perpendicular to the UV-laser polarization vector were produced by applying potentials to two segmented ring electrodes [33]. The field strengths were calibrated by measuring the Stark shift of the $40p_{3/2}$ Rydberg state and comparing it with the calculated Stark shift. The transition frequencies were measured after turning off the cooling lasers and MOT magnetic fields as explained in Ref. [33].

IV. RESULTS

Figure 2 shows millimeter-wave spectra of the $(38, 12, j^-, 1/2) \rightarrow (35, 13, j^-, 1/2)$ transition recorded at electric field strengths of (a) $F_1 = 5.60$ V cm^{-1}, (b) $F_2 = 7.51$ V cm^{-1}, (c) $F_3 = 8.47$ V cm^{-1}, and (d) $F_4 = 9.42$ V cm^{-1}. The lines have a full width at half maximum of 1.5 MHz, and their line centers can be determined with a precision of better than 100 kHz, see Tables I and II. Their center frequencies are indicated by full circles in panel (e), where they are compared to the frequencies calculated as explained above. This transition is an example of a type-II magic transition and corresponds to the situation depicted in Fig. 1(b). The strong dipole moment of the two states involved ($nk_{\mathrm{eff}} = 456$) implies that both states have large Stark shifts (up to ≈10 GHz), which are much larger than the bandwidth of 1 MHz of the UV-laser radiation used to prepare the $(38, 12, j^-, 1/2)$ initial state. The $(38, 12, j^-, 1/2) \leftarrow 4s_{1/2}$ transition exhibits a strong inhomogeneous broadening ($\Gamma_{\mathrm{FWHM}} = 28$ MHz at 10 V cm^{-1}) originating from the field inhomogeneity (≈0.3 V cm^{-2}) in the sample volume.

Because the linear Stark manifold has zero intensity for excitation from the $4s\,^2\mathrm{S}_{1/2}$ ground state at low fields, the measurements were only possible for fields $F > 5$ V cm^{-1}. The increase of the optically accessible p character with increasing field strength is reflected in the growing intensity of the $(38, 12, j^-, 1/2) \leftarrow 4s_{1/2}$ transition, as illustrated in Fig. 2(f), which shows the laser excitation spectra recorded at the fields used to record the millimeter-wave spectra. For the same reason, the signal-to-noise ratio of the corresponding millimeter-wave spectra also improves. The Stark shift of the two Rydberg states involved in the transition are more than 1000 times larger than the shift of the transition frequency.
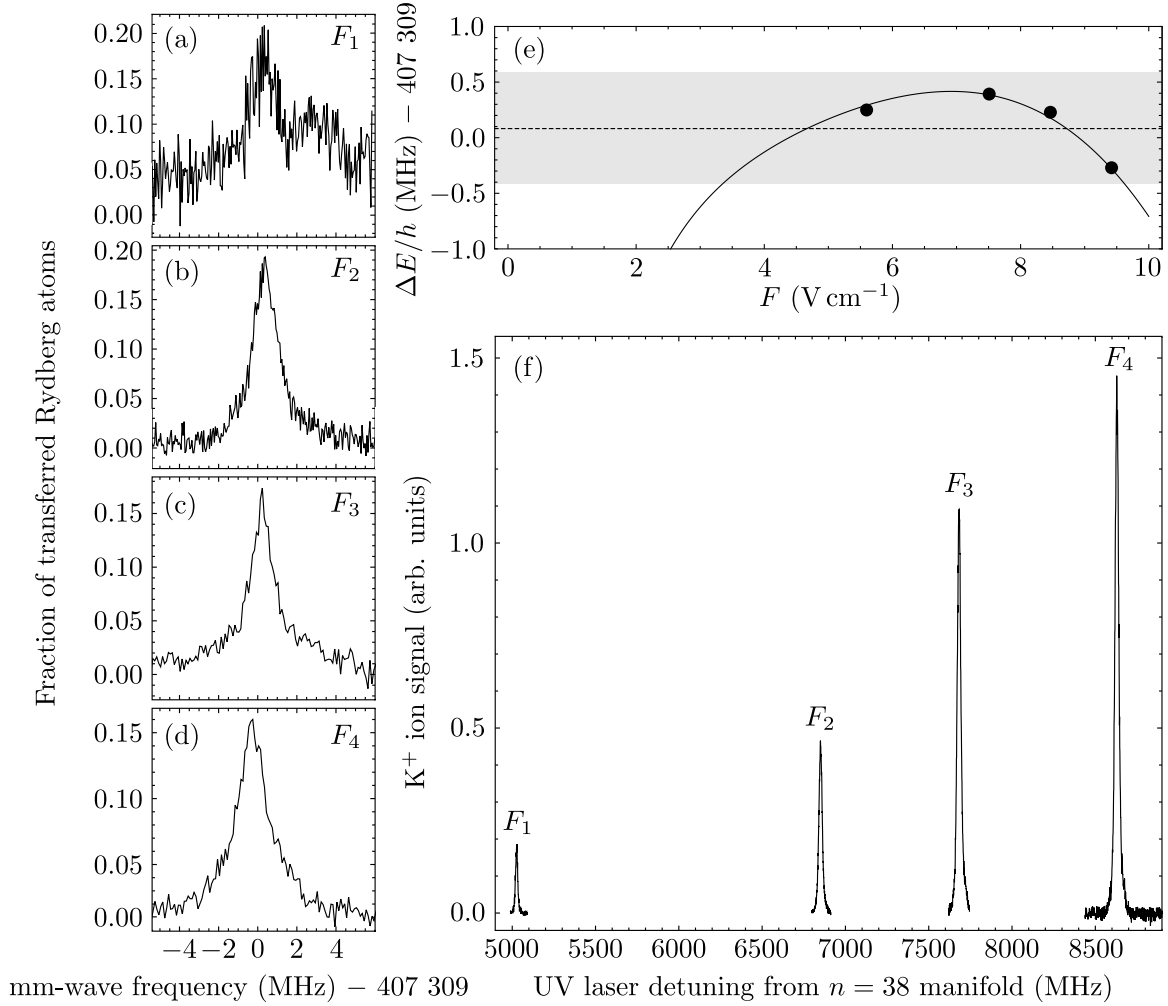
FIG. 2. Fraction of transferred Rydberg atoms for the $(38, 12, j^-, 1/2) \rightarrow (35, 13, j^-, 1/2)$ transition as a function of the millimeter-wave frequency in an electric field of (a) $F_1 = 5.60 \, \text{V cm}^{-1}$, (b) $F_2 = 7.51 \, \text{V cm}^{-1}$, (c) $F_3 = 8.47 \, \text{V cm}^{-1}$, and (d) $F_4 = 9.42 \, \text{V cm}^{-1}$. (e) Comparison of experimental (dots) and calculated (full line) transition frequencies. The dashed line and gray area represent the average frequency and the maximal deviation over the field range $(3.4–9.4 \, \text{V cm}^{-1})$. (f) UV-laser spectra of the $(38, 12, j^-, 1/2) \leftarrow 4s_{1/2}$ transition of ^{39}K recorded at the fields $F_1–F_4$.

The experimental and calculated transition frequencies are presented in Table I, which also gives the calculated Stark shifts of the two states. The horizontal dashed line in Fig. 2(e) gives the average calculated transition frequency $\tilde{\nu}_{\text{av}}$ in the field range between 3 and 10 V cm^{-1}.

$\Delta E_{\text{Stark}}^{\text{max}}/(h\sigma)$ is larger than 5000 in this field range with a maximal deviation of only 495 kHz at about 5.6 V cm^{-1} (see Table I). When using this transition as a magic transition in an

experiment the field range between 0 and 3 V cm^{-1} could be avoided by applying a background offset field.

Figure 3 depicts the measured field dependence of the transition connecting the central components of the Stark manifolds of $n = 40$ and $n = 42$, which is an example of a type-III magic transition [see Fig. 1(c)]. The transition could be measured over a larger field range (from 2.75 to 9.5 V cm^{-1}) than in the previous example because the p

TABLE I. Stark shifts of the Rydberg states involved in the $(38, 12, j^-, 1/2) \rightarrow (35, 13, j^-, 1/2)$ transition and comparison of observed and calculated transition frequencies for selected values of the electric-field strength.

F (V cm^{-1})	5.60(1)	7.51(1)	8.47(1)	9.42(1)
$\Delta E_{\text{Stark}}^{(38,12,j^-,1/2)}/h$ (MHz)	5071.609	6820.252	7699.287	8569.064
$\Delta E_{\text{Stark}}^{(35,13,j^-,1/2)}/h$ (MHz)	5057.954	6806.503	7685.747	8555.978
ν_{calc} (GHz)	407.309306	407.309400	407.309191	407.308737
ν_{exp} (GHz)	407.309249(31)	407.309392(11)	407.309228(18)	407.308730(15)
$\nu_{\text{exp}} - \nu_{\text{calc}}$ (kHz)	−57	−8	37	−7

TABLE II. Stark shifts of the Rydberg states involved in the $(42, 0, j^+, 3/2) \rightarrow (40, 0, j^+, 1/2)$ transition and comparison of observed and calculated transition frequencies for selected values of the electric-field strength.

F (V cm^{-1})	2.72(1)	3.68(1)	5.60(1)	7.51(1)	9.42(1)
$\Delta E_{\text{Stark}}^{(42,0,j^+,3/2)}/h$ (MHz)	−21.929	−15.018	4.177	28.859	57.032
$\Delta E_{\text{Stark}}^{(40,0,j^+,1/2)}/h$ (MHz)	−28.161	−21.967	−4.346	19.103	47.181
ν_{calc} (GHz)	191.165018	191.165734	191.167308	191.168541	191.168637
ν_{exp} (GHz)	191.164571(55)	191.165307(22)	191.166813(11)	191.168232(8)	191.168252(13)
$\nu_{\text{exp}} - \nu_{\text{calc}}$ (kHz)	−447	−427	−495	−305	−386

character of the linear Stark manifold induced by an electric field of given strength rapidly increases with increasing n value. The analysis of the Stark shifts is presented in Table II. Although the states involved in this transition have much smaller Stark shifts than in the previous example, the transition-frequency shifts relative to the average frequency in the field range from 2 to 10 V cm^{-1} are slightly larger, up to 1.5 MHz, resulting in a reduction factor of $\Delta E_{\text{Stark}}^{\max}/(h\sigma)$ of 57 in this range. This second transition is slightly less magic than the previous one, but the initial state $(40, 0, j^+, 1/2)$ offers the advantages of having a much smaller absolute Stark shift than the $(38, 12, j^-, 1/2)$ state and, thus, of being more easily accessible from the ground state with a narrow-band UV laser.

The calculated and experimental frequencies presented in Tables I and II agree within less than 0.5 MHz. We believe that the remaining discrepancies originate from deviations of the quantum defects of the $l > 4$ Rydberg states from the values estimated from the K$^+$ core polarizability and relativistic energy corrections [31,34]. This good agreement confirms the validity of the calculation procedure and validates the σ values calculated for arbitrary transitions. The calculated σ values can, therefore, be used as criteria in the search for magic transitions in ^{39}K and other atoms and molecules. The ten most magic electric dipole transitions for ^{39}K in the field range up to 10 V cm^{-1} of each of the three types discussed in this paper are presented for the possible combination of l and m_j values in Tables A 1–9 of the Supplemental Material [35]. This field range restricts Rydberg-Rydberg magic transitions to n values below 50 and implies that most transition frequencies are be-

yond 100 GHz. Magic transitions of lower frequencies would involve higher-n values, which, in turn, restrict the maximal value of the electric field. For example, transition frequencies below 100 GHz would involve Rydberg states with $n > 50$. As an illustration, an inventory of ^{39}K Rydberg-Rydberg magic transitions in the field range from 0 to 1 V cm^{-1} is presented in Tables A 10–18 of the Supplemental Material [35].

V. CONCLUSION AND OUTLOOK

The results presented in this paper demonstrate the existence of electric-field-independent Rydberg-Rydberg transitions in ^{39}K for two of the three types identified in our study. The experimentally observed transition frequencies agree with the calculated ones to better than 500 kHz. We believe that the remaining discrepancies originate from uncertainties in the quantum defects of the high-l states. The experiments, thus, validate the calculations which, in turn, can be used to systematically generate an inventory of possible field-independent transitions. A list of some of the most attractive ones in ^{39}K is provided in the Supplemental Material [35], which illustrates that they cover a broad range of frequencies between 20 GHz and 3 THz and that the ranges of frequencies and fields depend on the selected range of n values.

With maximal Stark shifts of less than 1 MHz over field ranges of more than 5 V cm^{-1}, these transitions are ideally suited for experiments aiming at coupling Rydberg atoms and solid-state devices, dipole-blockade experiments, and possibly precision measurements of the Rydberg constant using Rydberg-Rydberg transitions [36].

Type-I magic transitions have not been observed experimentally, in some cases because their frequencies are in a range where we do not have suitable light sources and in the others because we cannot field ionize the relevant Rydberg states at present. Rapid progress in the development of quantum cascade lasers in the terahertz range [37,38] makes us confident that we will soon be able to also observe them.

Two applications of Rydberg-Rydberg magic transitions immediately come to mind: (i) In recent quantum-simulation experiments (see, e.g., Refs. [7,8]), Rydberg atoms are arranged spatially in a deterministic way. Magic transitions would enable one to exploit the orientational dependence of the dipole-dipole interaction without suffering from field inhomogeneities and spectral broadening. (ii) Their full potential can be realized in hybrid experiments in which Rydberg atoms or molecules are coupled to solid-state devices, such as transmission-line resonators or to cavities [6,9–16].
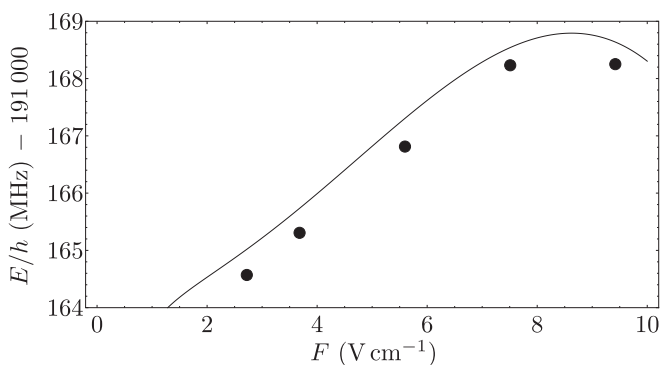

FIG. 3. Comparison of calculated Stark shift (full line) of the $(42, 0, j^+, 3/2) \rightarrow (40, 0, j^+, 1/2)$ transition of ^{39}K to the experimentally observed Stark shifts (full circles) as a function of the applied electric-field F.

[1] S. Haroche and J.-M. Raimond, *Exploring the Quantum: Atoms, Cavities and Photons* (Oxford University Press, Oxford, 2006).

[2] M. D. Lukin, M. Fleischhauer, R. Côté, L. M. Duan, D. Jaksch, J. I. Cirac, and P. Zoller, Phys. Rev. Lett. **87**, 037901 (2001).

[3] M. Saffman, T. G. Walker, and K. Mølmer, Rev. Mod. Phys. **82**, 2313 (2010).

[4] D. Petrosyan, G. Bensky, G. Kurizki, I. Mazets, J. Majer, and J. Schmiedmayer, Phys. Rev. A **79**, 040304(R) (2009).

[5] H. Weimer, M. Müller, I. Lesanovsky, P. Zoller, and H. P. Büchler, Nat. Phys. **6**, 382 (2010).

[6] S. D. Hogan, J. A. Agner, F. Merkt, T. Thiele, S. Filipp, and A. Wallraff, Phys. Rev. Lett. **108**, 063004 (2012).

[7] H. Labuhn, D. Barredo, S. Ravets, S. de Léséleuc, T. Macrì, T. Lahaye, and A. Browaeys, Nature (London) **534**, 667 (2016).

[8] J. Zeiher, J.-y. Choi, A. Rubio-Abadal, T. Pohl, R. van Bijnen, I. Bloch, and C. Gross, Phys. Rev. X **7**, 041063 (2017).

[9] P. Hyafil, J. Mozley, A. Perrin, J. Tailleur, G. Nogues, M. Brune, J.-M. Raimond, and S. Haroche, Phys. Rev. Lett. **93**, 103001 (2004).

[10] J. Mozley, P. Hyafil, G. Nogues, M. Brune, J.-M. Raimond, and S. Haroche, Eur. Phys. J. D **35**, 43 (2005).

[11] A. Tauschinsky, R. M. T. Thijssen, S. Whitlock, H. B. van Linden van den Heuvell, and R. J. C. Spreeuw, Phys. Rev. A **81**, 063411 (2010).

[12] H. Hattermann, M. Mack, F. Karlewski, F. Jessen, D. Cano, and J. Fortágh, Phys. Rev. A **86**, 022511 (2012).

[13] J. D. Carter and J. D. D. Martin, Phys. Rev. A **88**, 043429 (2013).

[14] T. Thiele, S. Filipp, J. A. Agner, H. Schmutz, J. Deiglmayr, M. Stammeier, P. Allmendinger, F. Merkt, and A. Wallraff, Phys. Rev. A **90**, 013414 (2014).

[15] C. Hermann-Avigliano, R. C. Teixeira, T. L. Nguyen, T. Cantat-Moltrecht, G. Nogues, I. Dotsenko, S. Gleyzes, J. M. Raimond, S. Haroche, and M. Brune, Phys. Rev. A **90**, 040502(R) (2014).

[16] H. Hattermann, D. Bothner, L. Ley, B. Ferdinand, D. Wiedmaier, L. Sárkány, R. Kleiner, D. Koelle, and J. Fortágh, Nat. Commun. **8**, 2254 (2017).

[17] T. F. Gallagher, *Rydberg Atoms* (Cambridge University Press, Cambridge, UK, 1994).

[18] M. T. Frey, X. Ling, B. G. Lindsay, K. A. Smith, and F. B. Dunning, Rev. Sci. Instrum. **64**, 3649 (1993).

[19] H. Hotop, D. Klar, J. Kreil, M.-W. Ruf, A. Schramm, and J. M. Weber, in *The 19th International Conference on the Physics of Electronic and Atomic Collisions*, AIP Conf. Proc. No. 360 (AIP, New York, 1995), p. 267

[20] A. Osterwalder and F. Merkt, Phys. Rev. Lett. **82**, 1831 (1999).

[21] T. Thiele, J. Deiglmayr, M. Stammeier, J. A. Agner, H. Schmutz, F. Merkt, and A. Wallraff, Phys. Rev. A **92**, 063425 (2015).

[22] R. P. Abel, C. Carr, U. Krohn, and C. S. Adams, Phys. Rev. A **84**, 023408 (2011).

[23] K. S. Chan, M. Siercke, C. Hufnagel, and R. Dumke, Phys. Rev. Lett. **112**, 026101 (2014).

[24] J. D. Carter, O. Cherry, and J. D. D. Martin, Phys. Rev. A **86**, 053401 (2012).

[25] L. A. Jones, J. D. Carter, and J. D. D. Martin, Phys. Rev. A **87**, 023423 (2013).

[26] Y. Ni, P. Xu, and J. D. D. Martin, Phys. Rev. A **92**, 063418 (2015).

[27] J. A. Sedlacek, E. Kim, S. T. Rittenhouse, P. F. Weck, H. R. Sadeghpour, and J. P. Shaffer, Phys. Rev. Lett. **116**, 133201 (2016).

[28] H. Katori, M. Takamoto, V. G. Pal'chikov, and V. D. Ovsiannikov, Phys. Rev. Lett. **91**, 173005 (2003).

[29] R. R. Ernst, G. Bodenhausen, and A. Wokaun, *Principles of Nuclear Magnetic Resonance in One and Two Dimensions* (Clarendon, Oxford, 1987).

[30] M. L. Zimmerman, M. G. Littman, M. M. Kash, and D. Kleppner, Phys. Rev. A **20**, 2251 (1979).

[31] M. Peper, F. Helmrich, J. Butscher, J. A. Agner, H. Schmutz, F. Merkt, and J. Deiglmayr, Phys. Rev. A **100**, 012501 (2019).

[32] M. Marinescu, H. R. Sadeghpour, and A. Dalgarno, Phys. Rev. A **49**, 982 (1994).

[33] H. Saßmannshausen, F. Merkt, and J. Deiglmayr, Phys. Rev. A **87**, 032519 (2013).

[34] C. J. Sansonetti, K. L. Andrew, and J. Verges, J. Opt. Soc. Am. **71**, 423 (1981).

[35] See Supplemental Material at https://link.aps.org/supplemental/10.1103/PhysRevA.100.032512 for a list of dc-field-magic Rydberg-Rydberg transitions in ^{39}K in the range of $20 \leqslant n \leqslant 50$ for electric fields between 0 and 10 V cm^{-1} and in the range of $50 \leqslant n \leqslant 90$ for electric fields between 0 and 1 V cm^{-1}.

[36] A. Ramos, K. Moore, and G. Raithel, Phys. Rev. A **96**, 032513 (2017).

[37] G. Scalari, C. Walther, M. Fischer, R. Terazzi, H. Beere, D. Ritchie, and J. Faist, Laser Photonics Rev. **3**, 45 (2009).

[38] L. Bosco, C. Bonzon, K. Ohtani, M. Justen, M. Beck, and J. Faist, Appl. Phys. Lett. **109**, 201103 (2016).